Dynamical properties and Wigner transitions of two-dimensional electron lattices on dielectric substrates

Lenac, Z.; Šunjić, Marijan

Source / Izvornik: **Physical Review B (Condensed Matter), 1991, 44, 11465 - 11471**

Journal article, Published version
Rad u časopisu, Objavljena verzija rada (izdavačev PDF)

https://doi.org/10.1103/PhysRevB.44.11465

Permanent link / Trajna poveznica: https://urn.nsk.hr/urn:nbn:hr:217:495313

Dynamical properties and Wigner transitions of two-dimensional electron lattices on dielectric substrates

Z. Lenac
Pedagogical Faculty, YU-51000 Rijeka, Croatia, Yugoslavia

M. Šunjić
Department of Physics, University of Zagreb, P.O. Box 162, YU-41001 Zagreb, Croatia, Yugoslavia

(Received 25 March 1991)

The dynamical properties (phonon spectrum, sound velocities, vibrational energy) and phase transitions of a two-dimensional Wigner lattice are discussed in a model that takes into account the perpendicular delocalization of electron wave functions. The lattice floats above the dielectric substrate (He,Ar), with the dielectric constant determining the image force on the lattice. Those two effects, the perpendicular electron delocalization and the dielectric image force, which are obviously correlated, were usually neglected in the previous discussions of the Wigner-lattice dynamics. Here we show their influence on the electron-electron interaction and consequently on the dynamical properties of the Wigner lattice. We also suggest an experimental situation where those effects in the phase diagram could be eventually studied and detected.

I. INTRODUCTION

Experimental evidence for a two-dimensional (2D) Wigner lattice of electrons formed above a dielectric (liquid-helium) surface[1] has revived interest for the physics of a Wigner crystal in the past decade. In our previous article[2] (hereafter referred to as I) we investigated electronic wave functions and energies in the Hartree approximation in order to derive the Wigner-lattice ground-state energy, which cannot be calculated satisfactorily in the model of a point-electron lattice on a dielectric surface. However, the dynamical properties of the lattice, such as dispersion relations, and sound velocities, which are used for the calculation of phase transitions, cannot be described properly in the Hartree approximation, which usually overestimates the electron energy.

In this article we take the results obtained in I as the starting point in deriving the dynamical properties of the Wigner lattice. Such calculations were already performed for a flat Wigner lattice on a dielectric surface with the dielectric constant $\epsilon=1$.[3] In our model we assume that electrons have finite extension in the direction perpendicular to the dielectric surface, while the dielectric is described by a constant that differs from unity. This leads to two closely related effects, because the larger dielectric constant of the substrate produces larger image force on the lattice electrons and therefore reduces their perpendicular delocalization. The perpendicular delocalization is also strongly correlated with the lateral electron density.[2]

In order to make our results more transparent, we shall apply our considerations to two dielectric substrates: helium with a low (static) dielectric constant ($\epsilon=1.055$) and argon with a relatively high dielectric constant ($\epsilon=1.660$). In both cases the electrons feel strong atomic repulsive potentials of the substrate due to the electronic excitation gap, and therefore those substrates can be suitable for the formation of a 2D Wigner lattice.

In Sec. II we formulate the problem and derive the total energy of the system. The eigenfrequencies of the system are obtained in Sec. III. They enable us to compare in Sec. IV the ground-state energy of the lattice in the present model with the results in I. In Sec. V we discuss the electronic lattice phase transition and the conclusions are given in Sec. VI.

II. MODEL HAMILTONIAN

The Hamiltonian that describes the electrons in a 2D Wigner lattice on a dielectric surface is[2]

$$H=\sum_i K_i+\sum_i W^{\rm im}(z_i)+\tfrac{1}{2}\sum_{j\neq i} W^{ee}(\rho_{ij};z_i,z_j)\ . \tag{1}$$

Here, $K_i=-\hbar^2\Delta_i/2m$ is the kinetic-energy operator and $W^{\rm im}(z_i)$ is the image potential of the electron i at a distance z_i above the dielectric surface. The interaction between the electrons (i,j) at a lateral distance $\rho_{ij}=|\boldsymbol{\rho}_i-\boldsymbol{\rho}_j|$ is described by $W^{ee}(\rho_{ij};z_i,z_j)$. The interaction between images is also included in W^{ee}, so the third term in Eq. (1) gives the total electron-electron interaction of a Wigner lattice (lattice potential).

In I we treated this Hamiltonian in the Hartree approximation. Here we shall make use of one important result derived in I, namely that the wave function of an electron in a Wigner lattice can be factorized into the lateral $v(\boldsymbol{\rho})$ and perpendicular $u(z)$ components:

$$\psi(\boldsymbol{\rho},z)=v(\boldsymbol{\rho})u(z) \tag{2}$$

and $(\boldsymbol{\rho},z)$ denote the lateral and perpendicular coordinates, respectively.

We assume that all electrons in the lattice are in their

"perpendicular ground state." Grimes *et al.*[4] have measured the perpendicular electron transitions to the excited (image potential) states for "free" 2D electrons on liquid helium and found the energy of the first excited state to be ≈ 126 GHz above the ground state. This corresponds to the temperature of ≈ 6.0 K. The electrons that are localized in a Wigner lattice, and particularly if they float on the substrate of a larger dielectric constant (e.g., argon), will obviously have larger binding energies. The phase transitions are measured typically at $T \lesssim 2$ K,[1,5] so we can assume that all electrons in the lattice will be in their "perpendicular ground state."

In the Wigner lattice the electron separation is typically larger than 100 Å, and usually $\gtrsim 1000$ Å,[1,5,6] so we can neglect the overlap of electron densities. The (perpendicular) ground-state wave function takes the form

$$u(z)=\prod_i u(z_i) , \tag{3a}$$

and the one-electron (Hartree) wave functions

$$u(z_i)=2\alpha^{3/2} z_i e^{-\alpha z_i} \tag{3b}$$

with the variational parameter α, which determines the electron perpendicular width $\langle \Delta z \rangle = \sqrt{3}/2\alpha$, are discussed in I. They are exact solutions of the Schrödinger equation for an electron in the image potential:

$$W^{\rm im}(z)=-\frac{e^2}{2}\int_0^\infty dk\, \beta e^{-2kz}=-\beta\frac{e^2}{4z} \tag{4}$$

with

$$\beta=\frac{\epsilon-1}{\epsilon+1}$$

and ϵ is the static dielectric constant of the substrate.

With the wave function (3), the total image energy of N electrons in the Wigner lattice becomes

$$E^{\rm im}=N\langle E^{\rm im}\rangle , \tag{5a}$$

where $\langle E_{\rm im}\rangle$ is the image energy of ith electron:

$$\langle E^{\rm im}\rangle=\int dz_i u^*(z_i)\left[-\frac{\hbar^2}{2m}\frac{\partial^2}{\partial z_i^2}+W^{\rm im}(z_i)\right]u(z_i)$$
$$=\frac{e^2}{2}a_0\alpha^2-\beta\frac{e^2}{4}\alpha . \tag{5b}$$

Here, a_0 is the Bohr radius.

The z-averaged lateral interaction between the two electrons at their sites $(\boldsymbol{\rho}_i,\boldsymbol{\rho}_j)$ is defined as[2]

$$\langle W^{ee}(\boldsymbol{\rho}_{ij})\rangle=\int |u(z_i)|^2\,|u(z_j)|^2 W^{ee}(\boldsymbol{\rho}_{ij};z_i,z_j)dz_i\,dz_j , \tag{6a}$$

$$W^{ee}(\boldsymbol{\rho};z,z')=\frac{A}{(2\pi)^2}\int d\mathbf{k}\, e^{i\mathbf{k}\cdot d\boldsymbol{\rho}} W(k;z,z') , \tag{6b}$$

$$W(k;z,z')=\frac{(2\pi)^2}{A}\frac{e^2}{2\pi k}(e^{-k|z-z'|}-\beta e^{-k|z+z'|}) . \tag{6c}$$

Therefore the total lattice potential becomes

$$W^{ee}=\tfrac{1}{2}\sum_i\sum_{j\,(\neq i)}\langle W^{ee}(\boldsymbol{\rho}_{ij})\rangle . \tag{6d}$$

The static part of this potential is due to the electrons in their regular positions $\boldsymbol{\rho}_i^0$ in the lattice:

$$W_0^{ee}=\tfrac{1}{2}N\langle w_0^{ee}\rangle , \tag{7a}$$

$$\langle w_0^{ee}\rangle=\sum_{j\neq i}\langle W^{ee}(\boldsymbol{\rho}_{ij}^0)\rangle . \tag{7b}$$

Now we can write the Schrödinger equation for the lateral part of the wave function in the form

$$H_{\rm osc}v(\boldsymbol{\rho})=(E-W_0^{ee}-E^{\rm im})v(\boldsymbol{\rho}) , \tag{8a}$$

where

$$H_{\rm osc}=-\sum_i\frac{\hbar^2}{2m}\frac{\partial^2}{\partial\rho_i^2}+W_h^{ee} \tag{8b}$$

and W_h^{ee} represents the dynamical part of the total lattice potential (6d). At low temperatures we can use the harmonic approximation, which gives the standard form for the oscillator energy of the Wigner lattice:

$$E_{\rm osc}=\int d\boldsymbol{\rho}\, v^*(\boldsymbol{\rho})H_{\rm osc}v(\boldsymbol{\rho})$$
$$=\sum_{\mathbf{k},p}(n_{\mathbf{k}p}+\tfrac{1}{2})\hbar\omega_p(\mathbf{k}) , \tag{9}$$

where $\omega_p(\mathbf{k})$ are the eigenfrequencies of the longitudinal (ω_+) and transverse (ω_-) lattice modes.

The same form (9) was obtained by Bonsell and Maradudin,[3] but they have neglected the perpendicular delocalization of the electron wave function (equivalent to taking $\alpha\to\infty$) and the influence of the substrate (i.e., $\beta=0$). Here we wish to discuss specifically the influence of these effects on the lattice eigenfrequencies and consequently on the Wigner phase transition.

We shall denote the $\alpha\to\infty,\beta=0$ limit as the classical (CL) approximation and the $\alpha\to\infty$ limit as the point-electron (PE) approximation.

III. DISPERSION RELATIONS

The eigenfrequencies $\omega_p(\mathbf{k})$ of the dynamical Wigner lattice are obtained in our model with the assumption that all the (lateral) collective modes have the same perpendicular delocalization. This procedure is justified because we have shown in I that α is almost independent of the spread (σ) (and therefore of the frequency ω) of the lateral wave function $v(\boldsymbol{\rho})$. Now we assume that α is independent of the electron frequency $\omega_p(\mathbf{k})$ in the whole first Brillouin zone. Therefore, instead of the lateral vibrations of the flat electron lattice, we dicuss the lateral vibrations of the delocalized perpendicular electron "strings."

In deriving the eigenfrequencies $\omega_p(\mathbf{k})$ we shall follow the procedure of Bonsell and Maradudin,[3] i.e., we shall use the fast-convergent Ewald transformation to perform the summation over all electrons. However, as in I, we have to extend this procedure in order to include our more complicated type of potential. The calculations are performed in Appendix A. The Appendix A in I is here referred to as Appendix AI.

The dispersion relations $\omega_\pm(\mathbf{k})$ for the hexagonal Wigner lattice of electrons on helium and argon substrates are shown in Fig. 1, along the boundaries of the ir-

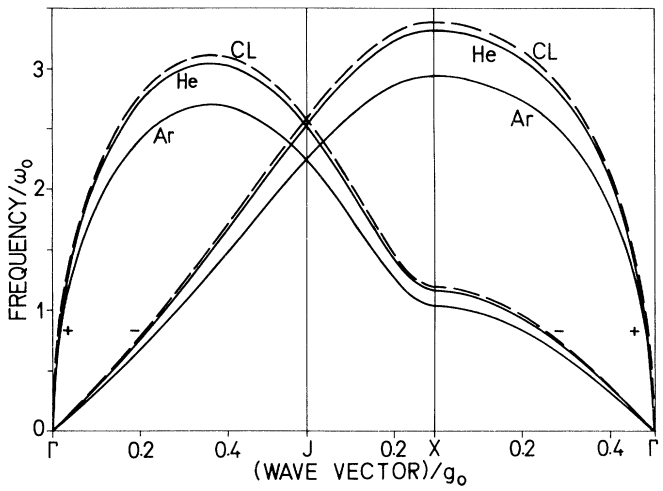

FIG. 1. Dispersion relations of the two vibrational ("phonon") modes for the 2D hexagonal lattice, on He and Ar. The lattice parameter is $r_0=300$ Å and the α values are taken from I: $4\alpha a_0=0.112$ for He, $4\alpha a_0=0.253$ for Ar, and $\alpha\to\infty$ for the CL curve. The frequencies $\omega_\pm$ are shown in the units $\omega_0=(e^2/mr_0^3)^{1/2}$ and the wave vectors $\mathbf{k}$ in units of the reciprocal-lattice vector $g_0=(4\pi/\sqrt{3})r_0$.

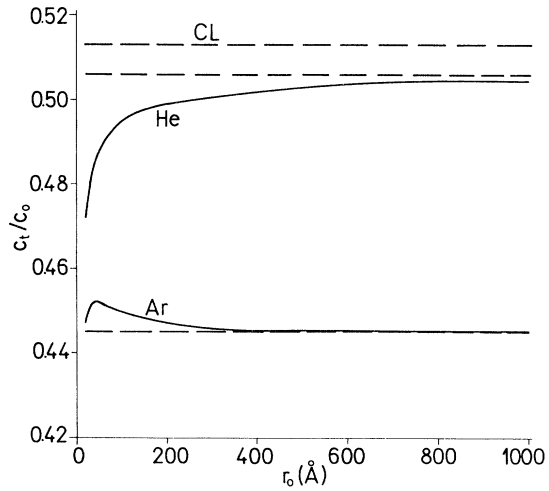

FIG. 2. The transverse vibrational velocities for the 2D hexagonal lattices on He and Ar substrates as functions of lattice parameter r_0, in units $c_0=\omega_0 r_0=(e^2/mr_0)^{1/2}$. The appropriate $\alpha(r_0)$ values for He and Ar are taken from I. The CL curve and the corresponding PE results are shown by dashed lines.

reducible element of the first Brillouin zone. When comparing these results to the CL model,[3] we find that the electron vibrational frequencies are reduced, particularly for argon. The main reason is the electron screening (image potential), which reduces the effective electron-electron repulsion.

The sound velocities of the transverse (c_t) and longitudinal (c_l) acoustic photons are

$$c_{l,t}=\lim_{k\to 0}\frac{\partial\omega_\pm}{\partial k} \tag{10}$$

and c_l (the slope of the ω_+ mode) diverges (see Appendix A). The divergency of c_l is the direct consequence of the lattice instability, and it cannot be removed by making a system neutral, e.g., by adding a metallic substrate infinitely far from the lattice. However, a metallic substrate close enough to the Wigner lattice will stabilize it by a strong image force exerted on its electrons, and as a consequence c_l becomes finite.[6]

Figure 2 shows c_t as a function of r_0 for He and Ar, together with the PE and CL approximations. In the $\alpha\to\infty$ limit, the function $f(x)$ [Eq. (A3b)] becomes a constant $(1-\beta)$ [(AI9)], which can be extracted from all T_j terms in (B16), giving

$$c_t(\alpha\to\infty)=0.513\sqrt{1-\beta}c_0\ . \tag{11}$$

From Fig. 2, we see that the PE approximation gives better results for c_t at larger r_0. Equation (11) becomes a good approximation for Ar at $r_0\gtrsim 400$ Å and for He at $r_0\gtrsim 1000$ Å, because the perpendicular electron width, and therefore the effect of perpendicular delocalization, is much greater in the He case.

IV. A COMPARISON OF STATIC AND DYNAMICAL HARTREE MODELS

In the present model we have found the energy of a Wigner lattice that takes into account the dynamical properties of the lattice electrons. Therefore, we shall call this a "dynamical Hartree model." It is a phonon model with the perpendicular "Hartree parameter" α. In I we found the ground-state energy of a lattice for the "static" electrons, i.e., in the "static Hartree model," and here we compare these two models.

The expressions for the image energy and the static part of the lattice potential are given by Eqs. (5) and (7), respectively. The vibrational energy of a Wigner lattice (9) (with the density parameter r_0) in the ground state is

$$E_{\rm osc}(r_0)=\tfrac{1}{2}\hbar\sum_p\sum_{\mathbf{k}}\omega_p(\mathbf{k})=\tfrac{1}{2}N\hbar\sum_p\langle\omega_p\rangle\ , \tag{12}$$

where we have defined

$$\langle\omega_p\rangle=\frac{1}{S_B}\int_{S_B}\omega_p(\mathbf{k})d^2k \tag{13}$$

and S_B is the surface of the first Brillouin zone.[3]

Therefore the total ground-state energy of the lattice (per one electron) in the dynamical model becomes

$$E_g=\sum_p\frac{\hbar}{2}\langle\omega_p\rangle+\langle E^{\rm im}\rangle+\tfrac{1}{2}\langle w_0^{ee}\rangle\ . \tag{14}$$

We evaluate $\langle\omega_p\rangle$ by integrating over the first Brillouin zone. This integration can be substituted by the summation over some special points in the zone:

$$\langle\omega_p\rangle=\sum_{i=1}^{L}a_i\omega_p(q_i)\ , \tag{15}$$

where the weights a_i and the special values of the wave

vectors q_i are given in Ref. 7, for $L=2$ and 6. We have taken $L=6$, which gives high enough accuracy for our purpose.

The results for $E_{\rm osc}(r_0)$ are shown in Fig. 3 for He and Ar, together with the PE result:

$$E_{\rm osc}=\tfrac{1}{2}N\hbar\times 4.28\sqrt{1-\beta}\omega_0 \ . \tag{16}$$

Although Figs. 2 and 3 look surprisingly similar, we should note that c_t and $\langle\omega_p\rangle$ have very different dependence on r_0 at large r_0: we find $c_t\sim c_0\sim r_0^{-1/2}$ and $\langle\omega_p\rangle\sim\omega_0\sim r_0^{-3/2}$.

In the static model,[2] the Hartree energy of an electron is

$$E_H=\langle\langle K_\parallel\rangle\rangle+\langle\langle E^{\rm im}\rangle\rangle+\langle\langle W^{ee}\rangle\rangle \ . \tag{17}$$

The double angular brackets denote that in the static approximation we have to average over both perpendicular and lateral directions. Obviously, $\langle\langle E^{\rm im}\rangle\rangle$ has the same form (5) as $\langle E^{\rm im}\rangle$ because the image potential is z dependent only, and the lateral kinetic energy is

$$\langle\langle K_\parallel\rangle\rangle=\frac{1}{N}\left\langle v(\boldsymbol{\rho})\left|-\frac{\hbar^2}{2m}\frac{\partial^2}{\partial\rho^2}\right|v(\boldsymbol{\rho})\right\rangle=-\frac{\hbar^2}{2m}\frac{1}{\sigma^2} \ , \tag{18}$$

where $v(\boldsymbol{\rho})$ is the harmonic-oscillator ground-state wave function.[2]

The average energy per one electron, which should be compared with Eq. (14), is

$$E_g=E_H-\tfrac{1}{2}\langle\langle w^{ee}\rangle\rangle \tag{19}$$

because we have to eliminate the double counting in the lattice potential $\langle\langle w^{ee}\rangle\rangle$. Notice that $\langle w^{ee}\rangle$ is equal to $\langle\langle w^{ee}\rangle\rangle$ with $\sigma=0$, so both these terms were already calculated in I.

In Fig. 4 we show our results for both dynamical and static Hartree models. The result is obvious: the dynamical model gives lower energy because it takes into account the formation of the Wigner lattice properly. However, the static Hartree model also gives surprisingly good results, particularly for He.

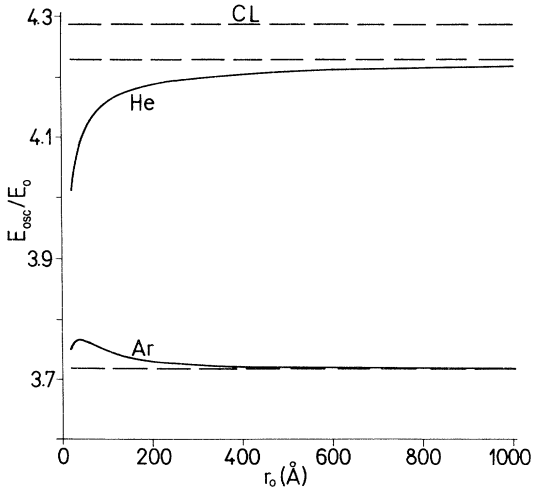

FIG. 3. The vibrational energies $E_{\rm osc}$ of 2D hexagonal lattices on He and Ar substrates, as functions of lattice parameter r_0 and in units of $E_0=\frac{1}{2}N\hbar\omega_0$. The CL curve and the corresponding PE results are shown by dashed lines.

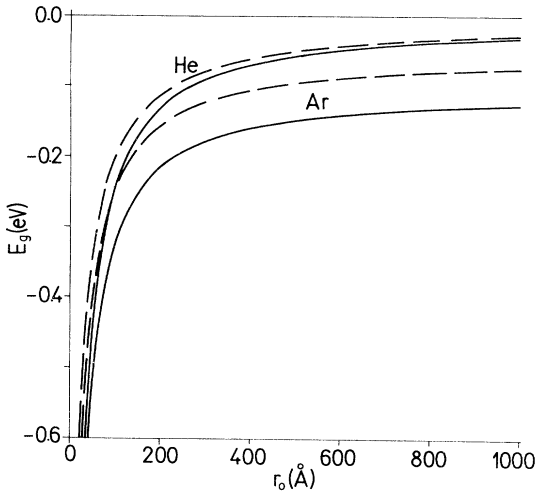

FIG. 4. The total ground-state energy per one electron for 2D hexagonal lattices on He and Ar substrates, as functions of lattice parameter r_0. Dynamical model, solid lines; static model, dashed lines.

V. THE PHASE TRANSITION: MELTING OF THE WIGNER LATTICE

It is widely accepted that the phase transition of a Wigner crystal can be described by the Kosterlitz and Thouless[8,9] and Halperin and Nelson[10] and Young[11] (KTHNY) theory. According to this theory the melting temperature T_m of the Wigner lattice is defined by[12]

$$k_BT_m=\frac{e^2}{r_0}\frac{1}{2\pi\sqrt{3}}\frac{c_t^2}{c_0^2}\left[1-\frac{c_t^2}{c_l^2}\right] \ . \tag{20}$$

With the bare Coulomb potential $V_0=e^2/r_c$, where r_c is the average electron distance [$r_c=(\sqrt{3}/2\pi)^{1/2}r_0$ for the hexagonal lattice], one can write Eq. (20) in the form

$$\Gamma^{-1}\equiv\frac{k_BT_m}{V_0}=\Gamma_0^{-1}F \ , \tag{21}$$

where

$$\Gamma_0=[(2\pi)^3\sqrt{3}]^{1/2}/(c_{t0}/c_0)^2 \ , \tag{22}$$

$$F=(1-c_t^2/c_l^2)c_t^2/c_{t0}^2 \ , \tag{23}$$

and $c_{t0}=0.513c_0$ is the CL transverse sound velocity (11). Using this result, Thouless obtained $\Gamma_0=79$,[9] while Grimes and Adams concluded from experiment that $\Gamma_0=137$.[1] This discrepancy was explained theoretically as a result of the temperature dependence of the sound velocity[13,14] and the anharmonic effects in the electron lattice.[15] Obviously, all those effects should be included

when studying the influence of electron delocalization, and we shall take them into account semiempirically by assuming that they change the bare value of Γ_0, Eq. (22), to its renormalized value $\Gamma_0=137$. Therefore, the difference between the CL and our theory is contained in the function F, Eq. (22b). Notice that in Sec. III we have found $c_l=\infty$, which gives $F=(c_t/c_{t0})^2$, and the ratio $c_t/c_0=0.513c_t/c_{t0}$ is shown in Fig. 2.

Following Ref. 6 we shall define the characteristic temperature T_0 and concentration n_0 in terms of parameter Γ_0:

$$n_0=\frac{4}{\pi}\frac{1}{(a_0\Gamma_0)^2},\quad k_BT_0=\frac{e^2}{a_0}\frac{2}{\Gamma_0^2}\ . \tag{24}$$

In these units the melting temperature (21) takes a simple form

$$\frac{T_m}{T_0}=\left[\frac{n}{n_0}\right]^{1/2}F\ . \tag{25}$$

We expect the KTHNY theory to be applicable in the classical regime $T<T_F$, where the Fermi temperature T_F for the 2D electron gas is given by[16]

$$\frac{T_F}{T_0}=2\frac{n}{n_0}\ . \tag{26}$$

Some authors[6,16] extrapolated the KTHNY theory to the quantum regime $T>T_F$ by simply substituting $k_BT_m\rightarrow K_m$, where K_m is the kinetic energy of the 2D electron gas at the melting temperature. However, this step is theoretically questionable and it would be very important to find its experimental confirmation (or refutation), which is still lacking. The main experimental problem is in achieving the Wigner lattice of high enough electron concentration, for the quantum regime $T>T_F$.[6]

One could further interchange the bare Coulomb potential V_0 in Eq. (21) with the total potential V felt by an electron in a Wigner lattice,[6,16,17] thus transforming Eq. (21) into Lindeman's melting criterion[18] $K_m/V=\Gamma^{-1}$. However, since the parameter $\Gamma=\Gamma_0/F$ also depends upon the total potential V through the sound velocity c_t, we believe that the substitution $V_0\rightarrow V$ amounts to "double counting," as was pointed out in Ref. 19.

Figure 5 shows the phase diagrams of the Wigner lattices on He and Ar substrates, together with the CL result. Notice that the experimental values of Grimes and Adams[1] for T_m fall in the low-temperature region $T\leq 0.03T_0\approx 1$ K, which is enlarged in the inset. From those values, Grimes and Adams obtained $\Gamma_0=137$ within the CL theory, so, because in this region the He curve is very close to the CL curve, we should take the same value for Γ_0 to recover the experimental data. We have taken the same value for Γ_0 for argon, because we have assumed that the influence of the substrate is taken into account through the function F. The argon curve differs appreciably from the CL curve due mainly to the higher image attraction of the argon substrate.

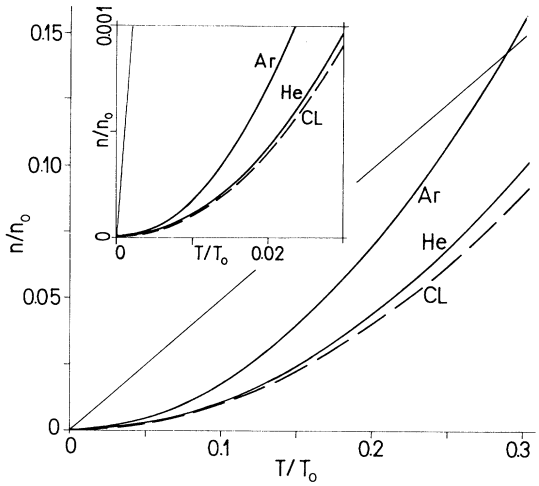

FIG. 5. Phase diagrams for the Wigner crystallization on He and Ar substrates, compared with the CL result. The straight line represents the $T=T_F$ condition. We used $\Gamma_0=137$, which gives $T_0=33.6$ K and $n_0=2.42\times10^{12}$ cm^{-2}.

VI. CONCLUSION

We have calculated the dynamical properties of a Wigner lattice by taking into account the image screening due to the dielectric properties of the substrate, and the finite size of electron wave functions in the direction perpendicular to the dielectric surface. The first effect is not appreciable for helium with the dielectric constant close to 1, but becomes very important for substrates with a larger dielectric constant, such as argon. The second, finite-size effect becomes important at higher electron densities ($r_0<1000$ Å). As we have shown in I, the electron delocalization, given by Δz, increases with r_0, but the relative size $\Delta z/r_0$ decreases, so at very low densities the electrons still behave as point particles. The region of higher electron concentrations, which should be easier to obtain on a dielectric with a larger dielectric constant or on a dielectric with a metallic substrate,[6] is particularly interesting when discussing phase transitions of a Wigner lattice.

We have shown a significant difference between the melting temperatures of a Wigner lattice on helium and argon substrates as a consequence of different vibrational properties. The eventual experimental confirmation of the melting curve, e.g., for the argon substrate on Fig. 5, would give further strong support that the KTHNY mechanism is responsible for the melting of the Wigner crystal.

Finally we want to summarize the simple physical message of this paper and Ref. 1. For a 2D electron lattice we have found by an explicit calculation (i) the reduction of the 2D phonon energy as compared to the 2D Hartree energy, and (ii) the reduction of energy of the 2D lattice with extended electron densities in comparison with the strictly planar 2D lattice. We believe that these results and ideas should be fruitful and lead to relevant implications in discussing other properties of 2D lattices.

ACKNOWLEDGMENTS

This work was partially supported by the U.S.–Yugoslav Joint Board on Scientific and Technological Cooperation, Grant No. PN-851/NIST.

APPENDIX A: CALCULATION OF VIBRATIONAL FREQUENCIES

The eigenfrequencies of the lattice are solutions of the standard two-dimensional eigenequation:

$$D(\mathbf{k})\epsilon_p(\mathbf{k})=m\omega_p^2(\mathbf{k})\epsilon_p(\mathbf{k}) , \tag{A1}$$

where $\epsilon_p(\mathbf{k})$ are the polarization eigenvectors for the two (longitudinal and transverse) acoustic modes, and $D(\mathbf{k})$ is the dynamical matrix of the system in a 2D $\mathbf{k}$ space:[3]

$$D_{ij}(\mathbf{k})=\lim_{\rho_0\to 0}[S_{ij}(\mathbf{k})-S_{ij}(0)] , \tag{A2a}$$

$$S_{ij}(\mathbf{k})=-\sum_{l\neq 0}\frac{\partial}{\partial\rho_{0i}}\frac{\partial}{\partial\rho_{0j}}\langle W^{ee}(\boldsymbol{\rho}_{0l})\rangle l^{i\mathbf{k}\cdot\boldsymbol{\rho}_l} \tag{A2b}$$

and $\langle W^{ee}(\boldsymbol{\rho}_{0l})\rangle$ is defined by Eq. (6).

To evaluate the dynamical matrix (A2), we transform $\langle W^{ee}(\boldsymbol{\rho}_{0l})\rangle$ as in Appendix AI in I:

$$\langle W^{ee}(\boldsymbol{\rho}_{0l})\rangle=e^2\frac{2}{\sqrt{\pi}}\int_0^\infty dx\, e^{-(\rho_0-\rho_l)^2x^2}f(x) , \tag{A3a}$$

$$f(x)=\tfrac{1}{8}\int_0^\infty dy\left[(y^2+3y+3)-\beta\tfrac{1}{15}y^5\right]\times e^{-y}e^{-(x/2\alpha)^2y^2} . \tag{A3b}$$

Here we need only the $\sigma=0$ limit of Eq. (AI10).

We use the extended Ewald transformation to transform the direct lattice sum over $\boldsymbol{\rho}_l$ into a sum over reciprocal-lattice vectors $\mathbf{G}$:

$$\sum_l e^{-(\rho_0-\rho_l)^2x^2}e^{i\mathbf{k}\cdot\boldsymbol{\rho}_l}=\frac{1}{S}\frac{\pi}{x^2}\sum_{\mathbf{G}}e^{i(\mathbf{G}+\mathbf{K})\cdot\boldsymbol{\rho}_0}e^{-(\mathbf{G}+\mathbf{k})^2/4x^2} . \tag{A4}$$

Here, S is the average area per electron.

We divide the dynamical matrix (A2) into two parts: the long-range ($x<\eta$) contribution D_{ij}^G, where we perform the transformation (A4), and the short-range ($x>\eta$) contribution D_{ij}^R:

$$D_{ij}(\mathbf{k})=D_{ij}^R(\mathbf{k})+D_{ij}^G(\mathbf{k}) , \tag{A5a}$$

$$D_{ij}^R(\mathbf{k})=-e^2\frac{4}{\sqrt{\Pi}}\eta^3\times\sum_{l\neq 0}\sin^2(\tfrac{1}{2}\mathbf{k}\cdot\boldsymbol{\rho}_l)[\delta_{ij}\phi_{1/2}^R(\eta^2\rho_l^2)-2\rho_l^i\rho_l^j\phi_{3/2}^R(\eta^2\rho_l^2)] , \tag{A5b}$$

$$D_{ij}^G(\mathbf{k})=e^2\frac{\sqrt{\pi}}{S}\frac{1}{\eta}\sum_{\mathbf{G}}[(\mathbf{G}+\mathbf{k})_{ij}\phi_{-1/2}^G((\mathbf{G}+\mathbf{k})^2/4\eta^2)-G_iG_j\phi_{-1/2}^G(G^2/4\eta^2)] . \tag{A5c}$$

The functions $\phi_n^{R,G}$ are the generalized Misra functions (AI14):

$$\phi_n^R(z)=\int_1^\infty dt\, t^n e^{-zt}f(\eta\sqrt{t}) , \tag{A6a}$$

$$\phi_n^G(z)=\int_1^\infty dt\, t^n e^{-zt}f(\eta/\sqrt{t}) , \tag{A6b}$$

and the parameter η is chosen to be (AI15)

$$\eta=(g_0/2r_0)^{1/2} . \tag{A7}$$

From Eq. (A1), the frequencies of the two modes are

$$\omega_\pm(\mathbf{k})=\omega_0 k\left[\frac{r_0}{2a_0}\right](T_+\pm\sqrt{T_-^2+4T_0^2})^{1/2} , \tag{A8}$$

$$T_\pm=\frac{2r_0}{e^2k^2}(D_{xx}\pm D_{yy}) , \tag{A9a}$$

$$T_0=\frac{2r_0}{e^2k^2}D_{xy} . \tag{A9b}$$

Let us determine the $\omega_\pm(\mathbf{k})$ in the long-wavelength ($\mathbf{k}\to\mathbf{0}$) limit. Following Eq. (A5) we first divide the terms T_j ($j=+,-,0$) into the short-range T_j^R and long-range T_j^G contributions:

$$T_j(\mathbf{k})=T_j^R(\mathbf{k})+T_j^{G\neq 0}(\mathbf{k})+T_j^{G=0}(\mathbf{k}) . \tag{A10}$$

Here we have extracted the $G=0$ term from T_j^G:

$$T_j^{G=0}(\mathbf{k})=\frac{2\sqrt{\pi}r_0}{S\eta}a_j(\varphi_{\mathbf{k}})\phi_{-1/2}^G(k^2/4\eta^2) ,$$

$$\left.\begin{matrix}a_+(\varphi)\\ a_-(\varphi)\\ a_0(\varphi)\end{matrix}\right\}=\begin{cases}1\\ \cos(2\varphi_{\mathbf{k}})\\ \sin(2\varphi_{\mathbf{k}}/2)\end{cases} , \quad \varphi_{\mathbf{k}}=\sphericalangle(\mathbf{k},x\text{ axis}). \tag{A11}$$

In the $\mathbf{k}\to\mathbf{0}$ limit

$$T_j^R(\mathbf{k}\to\mathbf{0})=\frac{4}{\sqrt{\pi}}\eta r_0\times\sum_{l\neq 0}Y_l(\hat{\mathbf{k}}\cdot\hat{\boldsymbol{\rho}}_l)^2[-\phi_{1/2}^R(Y_l)\delta_{j,+}+Y_l a_j(\varphi_l)\phi_{3/2}^R(Y_l)] , \tag{A12a}$$

$$T_j^{G\neq 0}(\mathbf{k}\to\mathbf{0})=\frac{2\sqrt{\pi}r_0}{\eta S}\times\sum_{\mathbf{G}\neq 0}[a_j(\varphi_k)\phi_{-1/2}^G(Y_G)-b_jY_G\phi_{1/2}^G(Y_G)+a_j(\varphi_{\mathbf{G}})(\hat{\mathbf{k}}\cdot\hat{\mathbf{G}})^2Y_G^2\phi_{3/2}^G(Y_G)] . \tag{A12b}$$

Here a caret denotes unit vectors,

$$Y_l=(\eta\rho_l)^2, \quad Y_G=(G/2\eta)^2 ,$$

the angles are

$$\varphi_l \sphericalangle(\boldsymbol{\rho}_l, x \text{ axis}) , \quad \varphi_{\mathbf{G}}=\sphericalangle(\mathbf{G}, x \text{ axis}) ,$$

and

$$\left.\begin{matrix} b_+ \\ b_- \\ b_0 \end{matrix}\right\} = \begin{cases} 4(\hat{\mathbf{k}}\cdot\hat{\mathbf{G}})^2+1 \\ 4(\hat{\mathbf{k}}\cdot\hat{\mathbf{G}})\cos(\varphi_{\mathbf{k}}+\varphi_{\mathbf{G}})+\cos(2\varphi_{\mathbf{G}}) \\ 2(\hat{\mathbf{k}}\cdot\hat{\mathbf{G}})\sin(\varphi_{\mathbf{k}}+\varphi_{\mathbf{G}})+\sin(2\varphi_{\mathbf{G}})/2 \end{cases} .$$

The terms $T_j^R(\mathbf{k}\to\mathbf{0})$ and $T_j^{G\neq 0}(\mathbf{k}\to\mathbf{0})$ remain finite. The $T_j^{G=0}(\mathbf{k}\to\mathbf{0})$ terms (A11) contain the $\phi^G_{-1/2}(0)$ function, which can be written as

$$\phi^G_{-1/2}(0)=\int_0^\infty dt \frac{1}{\sqrt{t}} f(\eta/\sqrt{t})=2\eta\int_0^\eta dx\, f(x)/x^2 . \tag{A13}$$

As discussed in Appendix AI, the integral in (A13) diverges for $\beta<1$. The divergent ($\mathbf{k}\to\mathbf{0}$) terms in Eq. (A8) are canceled for the combination of T's with the negative sign in the small parentheses while for the other combination one obtains

$$\lim_{k\to 0}[T_+ +(T_-^2+4T_0^2)^{1/2}]\sim\phi^G_{-1/2}(k\to 0)\sim 1/k . \tag{A14}$$

From Eqs. (A8), (A12), and (A14) we find

$$\omega_+(\mathbf{k}\to\mathbf{0})\sim\sqrt{k} , \quad \omega_-(\mathbf{k}\to\mathbf{0})\sim k , \tag{A15}$$

which gives for the sound velocities (10) an infinite value for c_l and a finite value for c_t:

$$c_t=\omega_0\frac{r_0}{2a_0}[T'_+(k=0)-\cos(2\varphi_{\mathbf{k}})T'_-(k=0) -2\sin(2\varphi_{\mathbf{k}})T'_0(k=0)]^{1/2} . \tag{A16}$$

Here, $T'_j\equiv T_j^R+T_j^{G\neq 0}$.

[1] C. C. Grimes and G. Adams, Phys. Rev. Lett. **42**, 795 (1979).
[2] Z. Lenac and M. Šunjić, Phys. Rev. B **43**, 6049 (1991).
[3] L. Bonsall and A. A. Maradudin, Phys. Rev. B **15**, 1959 (1977).
[4] C. C. Grimes, T. R. Brown, M. L. Burns, and C. L. Zipfel, Phys. Rev. B **13**, 140 (1976).
[5] H. W. Jiang, M. A. Stan, and A. J. Dahm, Surf. Sci. **196**, 1 (1988).
[6] F. M. Peeters, Phys. Rev. B **30**, 159 (1984).
[7] S. L. Cunningham, Phys. Rev. B **10**, 4988 (1974).
[8] J. M. Kosterlitz and D. J. Thouless, J. Phys. C **6**, 1181 (1973).
[9] D. J. Thouless, J. Phys. C **11**, 1189 (1978).
[10] D. R. Nelson and B. I. Halperin, Phys. Rev. B **19**, 2457 (1979).
[11] P. Young, Phys. Rev. B **19**, 1855 (1979).
[12] M. Šunjić and Z. Lenac, Europhys. Lett. **11**, 431 (1990).
[13] R. H. Morf, Phys. Rev. Lett. **43**, 931 (1979).
[14] D. S. Fisher, Phys. Rev. B **26**, 5009 (1982).
[15] M. C. Chang and K. Maki, Phys. Rev. B **27**, 1646 (1983).
[16] F. M. Peeters and P. M. Platzman, Phys. Rev. Lett. **50**, 2021 (1983).
[17] P. M. Platzman and H. Fukuyama, Phys. Rev. B **10**, 3150 (1974).
[18] F. Lindeman, Z. Phys. **11**, 609 (1910).
[19] M. Saitoh, Phys. Rev. B **40**, 810 (1989).